Synthesis of $Be_{12}Ti$ compound via arc melting or hot isostatic pressing

Ramil Gaisin[1,2], Vladimir Chakin[1], Rolf Rolli[1], Jan Hoffmann[1], Harald Leiste[1], Thomas Bergfeldt[1], Ute Jäntsch[1], Michael Klimenkov[1], Julia Lorenz[1], Aniceto Goraieb[3], Pavel Vladimirov[1], Anton Möslang[1]

[1]*Karlsruhe Institute of Technology, Institute for Applied Materials, Hermann-von-Helmholtz-Platz 1, 76344 Eggenstein-Leopoldshafen, Germany*

[2]*Institute for Metals Superplasticity Problems of RAS, Khalturina 39, 450001 Ufa, Russia*

[3]*Karlsruhe Beryllium Handling Facility, Hermann-von-Helmholtz-Platz 1, 76344 Eggenstein-Leopoldshafen, Germany*

Abstract

According to the recently proposed changes of the HCPB design concept of tritium breeding blanket for the DEMO fusion reactor, massive $Be_{12}Ti$ blocks are considered to be used for neutron multiplication. The paper compares two possible fabrication routes of solid beryllide blocks: combination of hot extrusion with arc melting or with hot isostatic pressing (HIP). Be-Ti composite rods produced by powder extrusion were chosen as a starting material. After arc melting, the ingot had cellular microstructure revealing mixture of $Be_{12}Ti$ and $Be_{10}Ti$ phases with considerable porosity. The powder metallurgy route, including extrusion and HIP, allows to achieve 98.6% of theoretical density and fine-grained $Be_{12}Ti$ microstructure with small amount of residual Be phase. EBSD analysis together with TEM showed that titanium beryllide has a grain size of 0.3–2.5 μm. It was observed that fine BeO particles are distributed along the grain boundaries and can pin them. Titanium beryllide after HIP has high microhardness of 1420 HV and fracture toughness of about 2.4 $MPa \cdot m^{1/2}$ comparable with that of many ceramics. The advantages of $Be_{12}Ti$ blocks manufacturing using extrusion and HIP are discussed.

Keywords: beryllide; intermetallic compound; hot isostatic pressing; arc melting; extrusion; DEMO.

ramil.gaisin@kit.edu

1. Introduction

Significant changes have been proposed recently in the design of the Helium Cooled Pebble Bed (HCPB) concept tritium-breeding blanket of the demonstration nuclear fusion power reactor power plant (DEMO) [1]. Firstly, $Be_{12}Ti$ was chosen as the neutron multiplier material, since titanium beryllide has an increased operating temperature, higher corrosion resistance, and significantly less swelling and tritium retention under irradiation [1-5]. Secondly, due to expected lower tritium residence time, titanium beryllide can be used in the form of massive blocks, instead of pebbles [1]. Low tritium trapping energies revealed in $Be_{12}Ti$ by ab initio modeling [6] in combination with the fact that in the neighborhood of each atom there is position where hydrogen isotope is not bounded, suggest that the limiting factor for the tritium release from titanium beryllide is its diffusion in the crystal lattice. Thus, an increase of the size of neutron multiplier from millimeters in pebbles to tens of centimeters in massive blocks will not lead to a significant tritium retention in beryllide. In addition, the density of the beryllide solid block (2.29 g/cm^3 [7]) is much higher than the density of the Be pebble blanket (1.85 g/cm^3 and packing factor γ=63.5% [8]), which compensates reduction of the beryllium fraction to 69.2% in $Be_{12}Ti$. Thus, switching from Be to $Be_{12}Ti$ logically leads to a change in the geometric dimensions and shape of the neutron multiplier material, in the newly developed design.

However, at the moment there is no industrial technology for manufacture of massive blocks of titanium beryllide. In the 1950s and 1960s, Brush Beryllium produced and tested small amounts of various beryllides as potential candidates for high temperature aerospace applications on the laboratory scale. Various methods of blended powders cold compaction, beryllide synthesis, grinding and final hot pressing were examined [9]. The obtained workpieces had high content of oxygen and other beryllides because of the need of complete grinding one or more additional times before final pressing [10]. Since better candidates for aerospace applications were found, industrial scale production of beryllides was not further pursued. Later, in the 2000s, about 60 kg of titanium beryllide were melted in Ulba Metallurgical plant, Kazakhstan. To this end zone melting was used to reduce the porosity and the shrinkage. Uranium and tantalum beryllides were also fabricated by the same producer using powder metallurgy methods. Laboratory-scale titanium beryllide ingots were cast in Japan using arc melting in argon atmosphere [3, 11]. Recently, the plasma sintering is used in Japan to produce titanium beryllide mainly in the form of electrodes for the subsequent pebbles manufacture by means of the rotating electrode method [3, 12-13]. Controlling the processing temperature and time, comparatively high quality material can be obtained [14-15]. The main disadvantages of the plasma sintering are higher porosity and the rapid heating and cooling rates of about 20–200 K/min.

The present paper compares two methods of titanium beryllide synthesis starting from the hot extruded rods fabricated from Be-Ti powder. The first method is arc melting, a simple and fast method of casting that provides high chemical homogeneity [16]. Powder metallurgical route based on hot isostatic pressing (HIP) was chosen as the second method of the synthesis. Microstructure and properties of material after different processing are compared with the aim to select the way of massive $Be_{12}Ti$ blocks industrial-scale production for their application as neutron multiplier in the DEMO fusion reactor.

2. Materials and experimental techniques

Be-Ti extruded composite rods were chosen as initial material for the investigation. The target composition is shown in Fig. 1 as $Be_{12}Ti$ (Be-7.7 at.% Ti or Be-30.8 wt.% Ti). Pure Be powder (>98% SP200F, Materion Corp. USA) and Ti powder (99,5% Alfa Aesar GmbH, Germany) with

ramil.gaisin@kit.edu

particle sizes of 32–45 μm were blended together and sealed into capsules at the Karlsruhe Beryllium Handling Facility (KBHF). The capsules were extruded at 650°C with reduction ratio of 8:1 at the Extrusion Research and Development Center, Technical University of Berlin. This temperature was selected to avoid formation of beryllides during extrusion, as they are too hard to be extruded homogeneously. Extrusion details are described in [17]. After extrusion Be-Ti composite rods with 12 mm in diameter were extracted from the capsules. Table 1 presents chemical composition of the as-extruded material. The samples were digested with acid in the graphite furnace and the elements subsequently analyzed with inductively coupled plasma optical emission spectrometry method (ICP-OES).

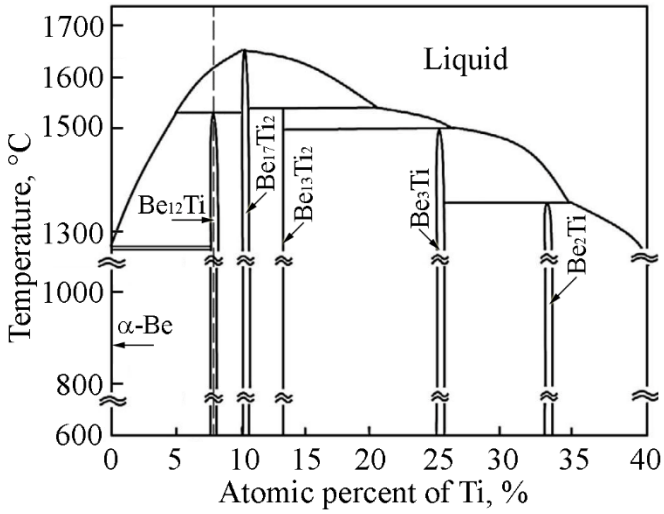

Fig. 1. A fragment of the Be-Ti phase diagram [18]. Dashed line indicates the composition under study

To transform extruded Be-Ti composite into beryllide, rod cuts were melted in a laboratory arc-melting furnace "Edmund Buehler" under argon atmosphere at the Institute for Metals Superplasticity Problems (IMSP RAS). To ensure higher homogeneity ingot was remelted four times. After casting the ingot was cooled at a rate of about 10–20 K/s. As result, 20-gram ingot was obtained in irregular shape with approximate dimensions of Ø30 mm × 7 mm. In the upper part ingot had a shrinkage.

Hot isostatic pressing (HIP) was chosen as a second way of titanium beryllide synthesis in the extruded powder composite. To do this, a section from a Be-Ti rod of 40 mm length was sealed again in a capsule and annealed at 1100°C under argon pressure of 102 MPa for 4 h in the "Edmund Buehler HIP 2000" gasostat (KBHF). Heating and cooling rates were about 10–20 K/min.

Table 1
Chemical compositions of extruded Be-Ti powder composite

%	Ti	O	Fe	C	Al	Mg	Si	N	Ca	U	Be
Wt.	29.11	0.219	0.102	0.077	0.037	0.036	0.022	0.0028	0.0018	0.00193	Bal.
At.	7.20	0.162	0.022	0.076	0.016	0.017	0.009	0.0024	0.0005	9.6E-05	Bal.

ramil.gaisin@kit.edu

Microstructure was examined using optical (OM, Reichert-Jung MeF3), scanning electron (SEM, Zeiss Merlin) and transmission electron microscopy (TEM, FEI Tecnai F20 and Talos F200X). After grinding the specimen surfaces were polished either mechanically or electrolytically. Due to toxicity of beryllium all preparation steps were done in gloveboxes. The polishing electrolyte was composed of H_3PO_4 (150 ml), H_2SO_4 (45 ml), and glycerol (45 ml). The volume fraction of phases was defined by the systematic point count method using mechanically polished specimens.

Electron backscatter diffraction (EBSD) and transmission Kikuchi diffraction (TKD) were used to examine microstructure features of titanium beryllide after HIP. The maps were built in surface normal-projected inverse pole figure (IPF-Z) orientation coloring. The black and white lines on the maps indicate high- and low-angle grain boundaries respectively. Energy-Dispersive X-Ray Spectroscopy (EDS) was used to analyze only titanium and oxygen content on SEM. Lamellae having about 25×10×4 μm^3 were lifted out from the specimen after HIP using focused ion beam (FIB) on a FEI Helios, Culham Centre for Fusion Energy, UK. Zeiss Auriga microscope was used for final polishing of lamellae windows of about 6×6×0.2 μm^3.

The composition of lamellae was examined using a Talos F200X transmission electron microscope (Thermo Scientific Company) equipped with a Super X-EDS system for energy-dispersive X-ray spectroscopy (EDX), a Gatan Infineon EELS spectrometer, and a scanning unit (STEM) with high-angle annular dark-field (HAADF) detector. Spatially resolved EDX analyses was performed in STEM mode.

X-ray diffraction (XRD) measurements were performed on Seifert PAD II diffractometer with Cu-$K\alpha_{1/2}$ radiation. Microhardness was measured on Zwick Roell Indentec ZHμ tester using 100-1000 gf indentation forces. Density was measured by the hydrostatic weighing in $C_{14}H_{30}$ liquid media (Mettler Toledo MS303TS).

3. Results and discussion

3.1. Initial extruded Be-Ti powder composite

According to XRD analysis (Fig. 2), the composite after extrusion consists of pure Ti and pure Be phases and no other phases were detected. Fig. 3 shows the microstructure of the composite along and across the extrusion direction. The microstructure is formed by Ti fibers (dark in OM and bright in SEM) elongated in extrusion direction in Be matrix. Cross sections (Fig. 3b,d) of these Ti-fibers have irregular shape. Fiber sizes are 2–40 μm in cross section and 10–60 μm in length. Volume fraction of the titanium phase is about 21% in both sections (Table 2). The prior particle boundaries (prior surfaces of powders) are not revealed in the extruded material apparently because of high degree of deformation during extrusion.

The EDS confirmed that the fibers consist of pure titanium (Fig. 4a), whereas almost no titanium is detected in the surrounding matrix. Beryllium cannot be reliably detected by EDS, since low energy characteristic X-ray of Be is known to be mostly absorbed by the sample. Higher oxygen content was detected on Be and Ti phase boundaries and inside of these phases (Fig. 4b). Oxygen enriched particles and areas are often arranged in stripes along the extrusion direction. This increased oxygen content is incorporated into the composite structure from the oxidized powder surfaces. Since beryllium is oxidized more strongly than titanium even at room temperature [9], higher oxygen content on the EDS maps highlights the prior particle boundaries of Be powder. Elemental EDS maps of other impurities (Fe, C, Al…) did not show any considerable spatial inhomogeneity and therefore are not presented in this work.

ramil.gaisin@kit.edu

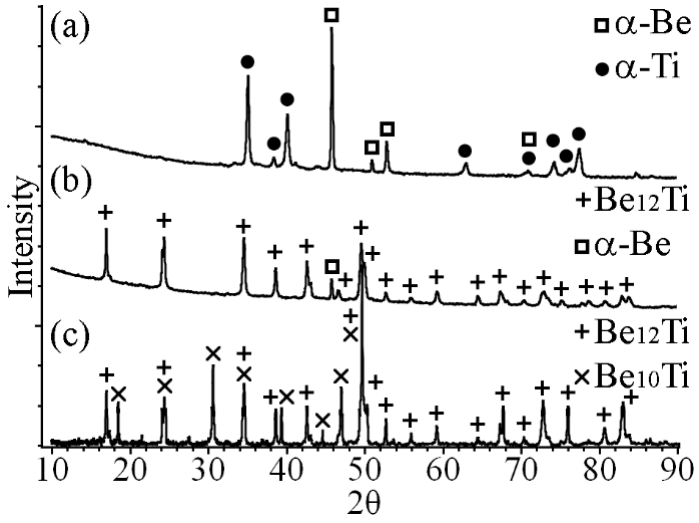

Fig. 2. X-ray diffraction patterns: (a) initial extruded Be-Ti composite, (b) after subsequent hot isostatic pressing, (c) after arc melting of extruded composite

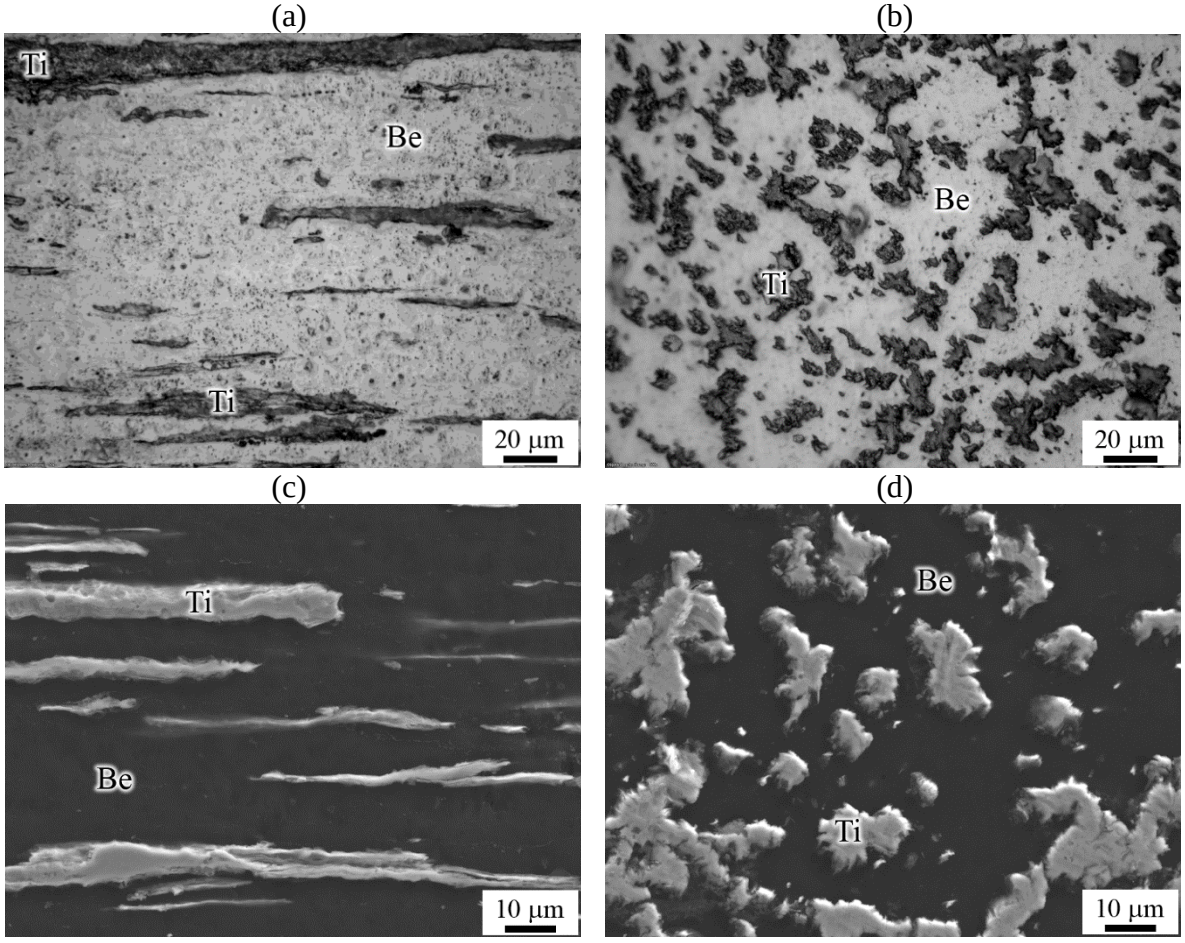

Fig. 3. Microstructure of Be-Ti composite after extrusion: (a,b) OM, (c,d) SEM; (a,c) along and (b,d) across extrusion direction

Microhardness measurements showed that both beryllium and titanium phases have similar microhardness of about 315–320 HV (Table 2). According to [9, 19], the hardness of pure Be

SP100C and SP200F after different treatment is about 160–170 HV (83.6–85.5 HRB). The hardness of titanium ranges within about 120–300 HV depending on impurities level [20]. In the reference [21], 99.5% purity titanium (the same purity titanium was used for composite preparation in this work) has the hardness of 265 HV. Higher hardness of both beryllium and titanium phases in the extruded composite can be explained by various hardening mechanisms during extrusion. No Be-Ti intermetallic phases were detected in the microstructure that could increase hardness (Fig. 2-3).

According to the hydrostatic weighing, the extruded Be-Ti composite has the density of 2.204 g/cm^3 (Table 2). Comparing calculated theoretical density (TD) of the Be-30.8wt.%Ti composite (2.231 g/cm^3) with pure Be and pure Ti phases, one can conclude that extrusion at 650°C with 8:1 reduction compacted material up to 97.6% of the TD.

Table 2.
Density, phase composition, volume fraction and microhardness of Be-Ti materials subjected to various processing

Processing	Density, g/cm^3	Phase	Volume fraction, %	Microhardness, HV 0.1
Extrusion	2.204	Be	79	320±20
		Ti	21	315±20
Arc melting	2.111	$Be_{12}Ti$+$Be_{10}Ti$	–	980±140
Extrusion and HIP	2.258	$Be_{12}Ti$	93	1420±40
		Be+porosity	7	360±30

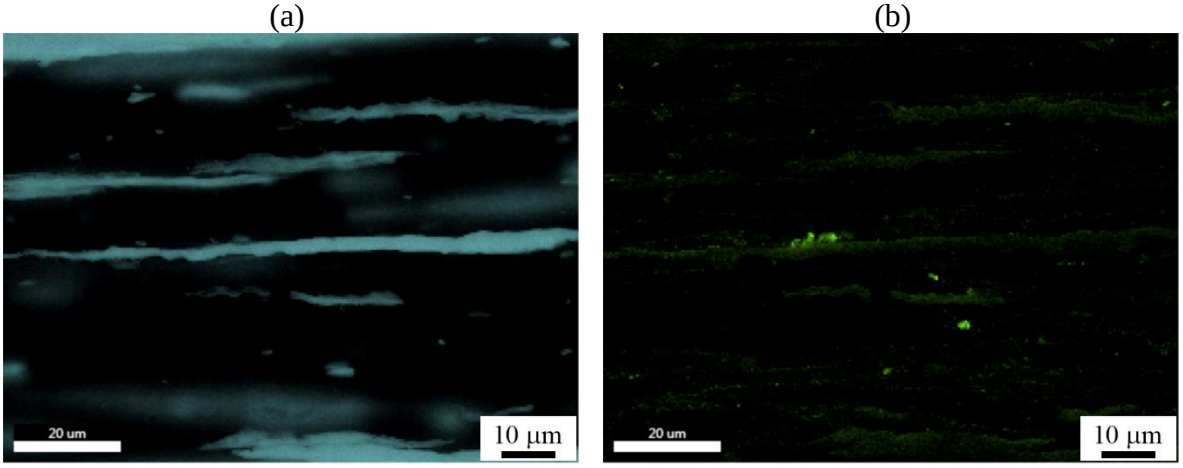

Fig. 4. Elemental EDS maps of extruded Be-Ti composite showing (a) titanium and (b) oxygen distributions

3.2. Arc melting of extruded Be-Ti composite

Using of unconsolidated powders for melting by the argon-arc method is possible, but it can lead to the blowing of powders by an argon arc and to the loss of material. Therefore, the extruded Be-Ti composite rods were chosen as a material for casting. The arc melting was accompanied by intense evaporation of beryllium. After initial heating of the composite up to melting, the reaction of beryllium and titanium proceeded spontaneously without additional heat supply. During subsequent remelting of the ingot intense beryllium evaporation complicated the melt flow and the

casting processes. Owing to this evaporation, the weight of the ingot decreased by 4.1% compared to the weight of the starting material.

XRD analysis performed for the as-cast alloy showed the presence of the target $Be_{12}Ti$ phase and additional peaks of $Be_{10}Ti$ phase (Fig. 2). The second phase is often not represented in the Be-Ti diagrams [9, 18]. However, this phase was observed in the cast Be-7Ti (at.%) alloy in [3]. $Be_{10}Ti$ is shown on Be-Ti diagram [22], but its structure remains unknown. This phase seems to emerge during argon arc melting as an intermediate phase in peritectic reactions during solidification. Assuming that the entire mass reduction during casting caused by beryllium evaporation, the resulting composition of the ingot should be Be-8.2 at.%Ti. The composition shift towards a higher amount of the titanium can explain the formation of the two-phase $Be_{12}Ti$+ $Be_{10}Ti$ microstructure during crystallization and cooling.

As-cast Be-Ti alloy has a cellular grain microstructure with an average size of 5–30 μm (Fig. 5). These grains resemble remnants of a dendritic structure and have pores at the boundaries, sometimes forming discontinuities and cavities especially in the upper part of the ingot (Fig. 5b). Similar porosity was observed in cast pebbles of titanium beryllide, obtained by the rotating electrode method [23]. The increased porosity in both cases can be explained by relatively fast cooling during the peritectic and eutectic reactions.

EDS showed that some cellular grains in the center have a higher amount of titanium than in the periphery (Fig. 5c). According to [3], the grain centers can be formed by the $Be_{10}Ti$ phase, and the edges by the $Be_{12}Ti$ phase, but both optical and scanning electron microscopies do not give a noticeable contrast between these phases. However, SEM in backscattered electrons of the same place as the EDS revealed difference in titanium content (Fig. 5d). Due to the impossibility of distinguishing $Be_{10}Ti$ and $Be_{12}Ti$ phases during microhardness measurements, the average microhardness has a large scatter and amounted to 980±140 HV. The obtained high hardness of beryllides is consistent with the results published in [3, 9, 24].

After casting the density of the alloy was measured as 2.111 g/cm^3 or 92% of theoretical density of $Be_{12}Ti$. Compared to the extruded composite, the density decreased, and this is consistent with the high porosity level in the cast alloy. It should be noted that similar low densities in cast materials were also observed in [3, 25]. Casting with slower cooling rates may result in a higher density and lower porosity. Due to composition deviation, the presence of two phases and higher porosity, further study of the cast material seems to be impractical.

ramil.gaisin@kit.edu

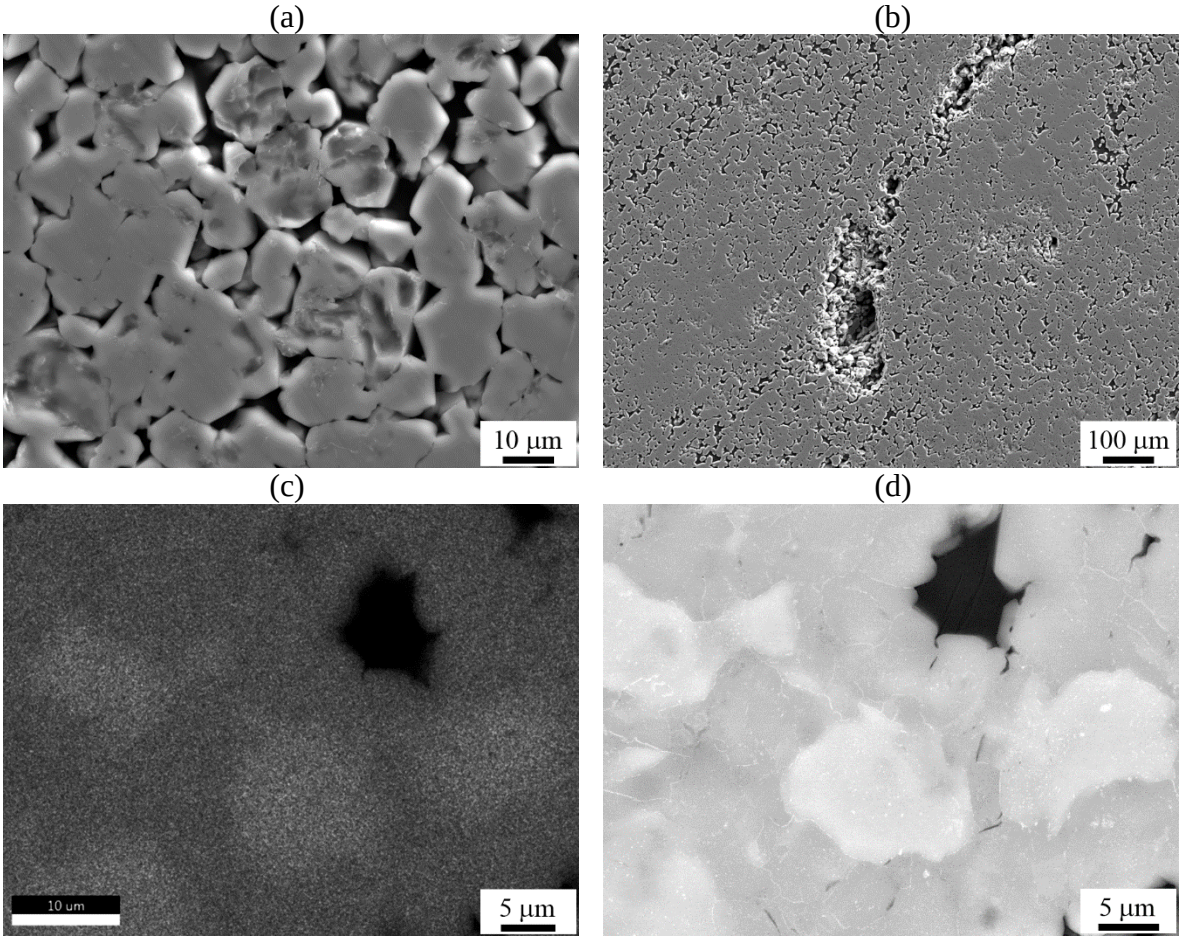

Fig. 5. Microstructure of the arc melted alloy: (a) porosity between grains, (b) cavity in the upper part of the ingot, (c,d) areas with a difference in titanium content; (a,b) SEM, (c) titanium EDS map, (d) SEM in backscattered electrons

3.3. Hot isostatic pressing of extruded Be-Ti composite

Generally compared with casting, powder metallurgy has several disadvantages. They are i) a higher content of impurities, ii) the complexity of manufacturing, iii) the increased cost. However, in the case of titanium beryllide casting, evaporation of beryllium, peritectic and eutectic reactions during crystallization led to a deviation of the chemical and phase composition as well as an increased porosity. Currently, powder metallurgy is the main processing route for metallic beryllium components production. This route provides better microstructure and higher mechanical properties while casting could only be used in cases where mechanical properties were not important [9]. A number of various beryllium powders are available on the market. Since the production of beryllide requires a large amount of beryllium, often offered in the powder form, it is reasonable to synthesize titanium beryllide using full powder metallurgical route.

Among the various methods of powders consolidating and the synthesis of beryllide, the HIP seems to be the most appropriate considering the potential industrial production. Compared to vacuum hot pressing HIP permits lower temperatures and higher pressures and provides smaller grain size with lower porosity [9]. Compared to plasma sintering methods HIP can provide higher density and allows low heating and cooling rates.

ramil.gaisin@kit.edu

The use of powders after cold compaction for HIP instead of extruded material is much cheaper and less time-consuming. The first experiments in KBHF showed that, despite annealing at a very high temperature up to 1350°C during HIP, the resulting material had high porosity and other phases in the composition [26]. Such high porosity is unacceptable for a blanket application, since tritium can be retained in pores and voids. The main disadvantage of cold compaction in KBHF is that the density of the powders after cold compaction can reach 80% of TD, even after pressing with the maximum possible load. Due to the joint deformation of Be and Ti powders during hot extrusion, the density reached 97.6% of TD. Therefore, it could provide lower porosity after HIP.

After extrusion and HIP of Be-Ti composite, $Be_{12}Ti$ phase peaks and small peak corresponding to beryllium are observed on the X-ray diffraction spectrum (Fig. 2c). According to the systematic point count method of mechanically polished samples, about 93% of the microstructure consists of $Be_{12}Ti$ phase elongated in the extrusion direction (Fig. 6, Table 2). On OM and SEM micrographs, these beryllide areas are "separated" from each other by stripes of fine particles. On the triple junctions of $Be_{12}Ti$ areas, residue beryllium phase is observed. Beryllium phase has higher porosity, which can be explained by the Kirkendall effect, emerging from the difference in diffusion rates of Be and Ti atoms. A similar increase in beryllium porosity after heat treatment was previously observed in the cast Be-Ti pebbles [23]. The density of the sample after HIP increased up to 2.258 g/cm^3 or 98.6% of $Be_{12}Ti$ TD (Table 2). The presence of residual beryllium phase with pores may explain the obtained density values lower than TD.

Fig. 7a,b represents EDS maps showing quite uniform Ti distribution and higher oxygen content on prior particle boundaries. After HIP these boundaries became clearly visible both in OM and SEM in comparison with the extruded composite, in which they were observed only using EDS. In addition, several Ti enriched areas up to 20 μm in diameter are observed (Fig. 7c). These areas often cause formation of microcracks and cracks extending hundreds of micrometers (Fig. 7d). Unfortunately, EDS did not show the exact composition of these Ti-enriched particles (no reliable data on Be content). These particles can be formed by other beryllides, e.g. Be_2Ti or $Be_{17}Ti_2$, which were observed between pure Ti and $Be_{12}Ti$ phases in [14, 27]. The increased content of titanium, the presence of Ti enriched regions and residual Be phase indicate that the time and temperature of HIP were not sufficient to accomplish diffusion of Ti and Be and to achieve their uniform distribution in the material. The cracks formation could be explained by the difference in the coefficients of thermal expansion of $Be_{12}Ti$ and other beryllides. That might cause high local stress during cooling after HIP.

ramil.gaisin@kit.edu

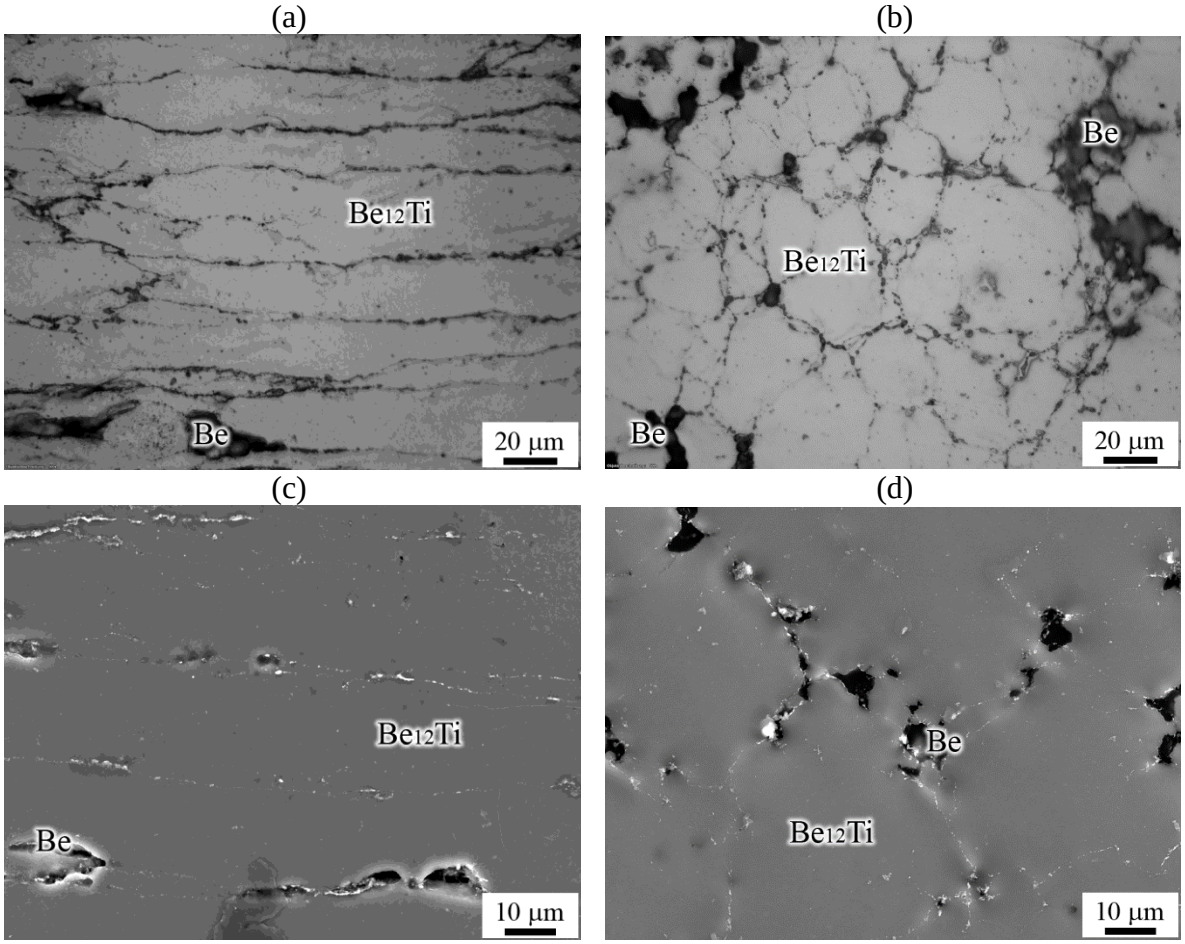

Fig. 6. Microstructure of Be-Ti composite after extrusion and hot isostatic pressing: (a,b) OM, (c,d) SEM; (a,c) along and (b,d) across extrusion direction

On SEM micrographs with an angle of 70 degrees and higher magnification, thin boundaries are observed inside the beryllide phase (Fig. 8a,b). Oxide particles having lengths of up to 5 μm lined up along the prior particle boundaries (Fig. 8a). The conducted EBSD analysis (Fig. 8c,d) along and across extrusion direction showed that $Be_{12}Ti$ is formed by fine nearly equiaxed grains with a mean grain size of 0.6–0.7 μm. Grains do not have a preferential orientation regarding to the direction of extrusion in both sections. Black undefined regions on the EBSD maps correspond to oxygen enriched particles on the prior particle boundaries, which in this case are not grain boundaries in contrast with other powder materials, where grains often have the initial powder particle sizes. In addition to fine grains, coarser grains reaching 2–2.5 μm in diameter are also observed, mostly far from the prior particle boundaries. Some of these grains have a number of subgrain boundaries inside marked with white lines on EBSD maps (Fig. 8c,d). But generally the fraction of high-angle grain boundaries after HIP is rather high and reaches 83–87%.

ramil.gaisin@kit.edu

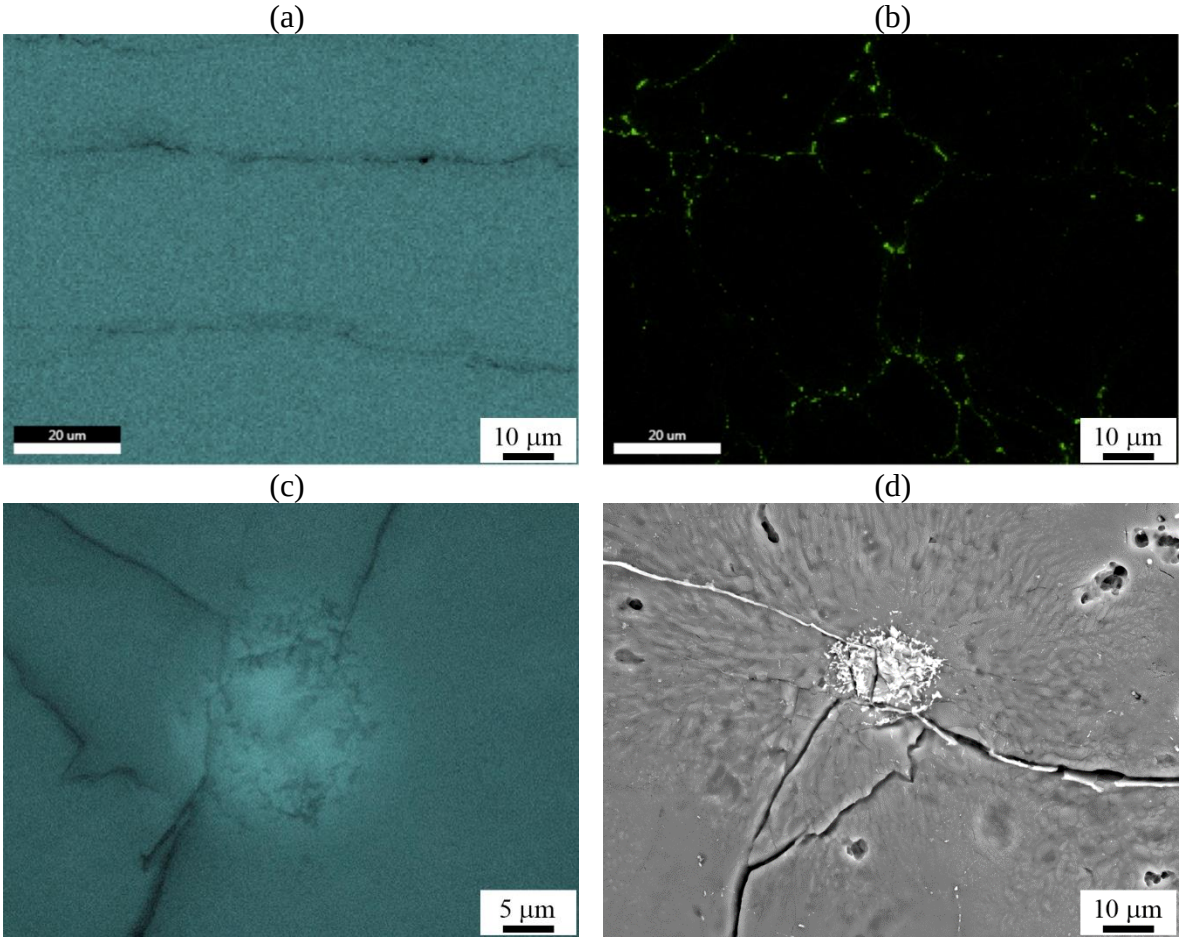

Fig. 7. (a-c) Elemental EDS maps and (d) SEM picture of Be-Ti composite after extrusion and hot isostatic pressing. (a, c) titanium, (b) oxygen distributions, (d) crack caused by Ti-enriched particle; (a) along and (b-d) across extrusion directions

For TEM investigation lamellae were lifted out from the sample after HIP using focused ion beam. Fig. 9 represents the process of Pt deposition before cut and the polished surface of the lamella using FIB. The lamellae were prepared from different microstructure features, in particular across the prior particle boundaries (Fig. 9a lamella 1) and inside the area between these boundaries (Fig. 9a lamella 2). On the polished surface of the lamella 1 prepared across the prior particle boundary one can see a number of small oxide particles together with relatively bigger particles of 0.2–1.5 µm in length.

EDS analysis in the STEM mode showed that the particles have higher oxygen content and no titanium (Fig. 10b,c). Using EELS, it was possible to detect beryllium and oxygen together in these particles. This suggests that the particles are formed by beryllium oxide and not titanium oxide. The beryllium oxide could be incorporated into the structure of the material under study from the surface of oxidized beryllium powder, which oxidizes much more strongly than titanium. The iron elemental maps show a higher iron content at the $Be_{12}Ti$ grain boundaries (Fig. 10a,d). EDS analysis in the SEM has lower sensitivity and did not show such distribution of iron, since average iron content is about 0.1 wt.% (Table 1).

ramil.gaisin@kit.edu

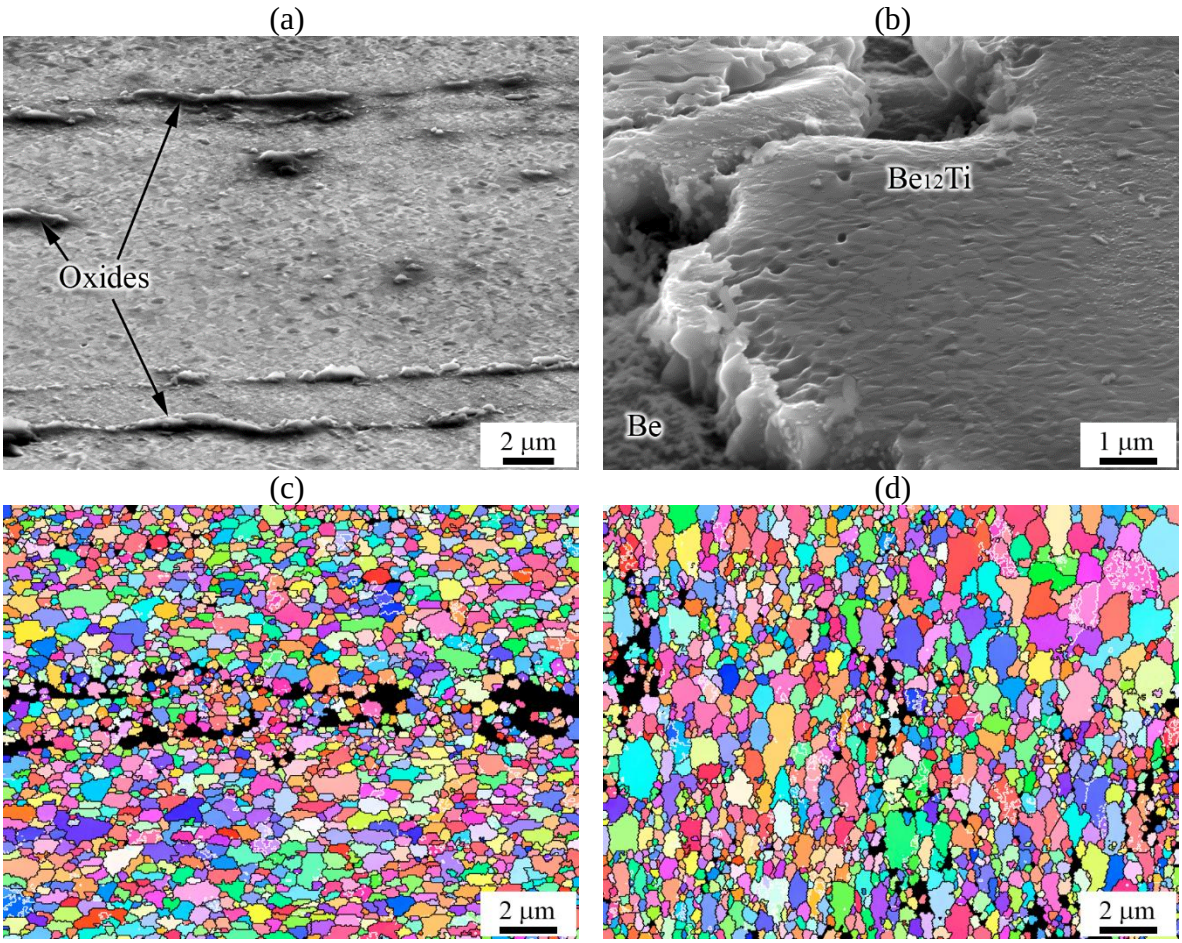

Fig. 8. Microstructure of Be-Ti composite after extrusion and hot isostatic pressing: (a,b) SEM with 70° view, (c,d) EBSD maps of $Be_{12}Ti$ phase; (a,c) along and (b,d) across extrusion direction. Black areas on the EBSD maps correspond to oxide particles on prior particle boundaries.

After polishing of the lamella, TKD together with TEM (Fig. 11a,b) confirmed that $Be_{12}Ti$ phase consists of small grains of 0.3–1 μm in diameter. The same grain structure was found both using TEM and TKD. Corresponding grains are marked with capital letters on the pictures. The grains are randomly oriented (Fig. 11a). The grains presumably have high internal stress, which result in the formation of numerous intergranular defects. Some of these defects are visible as sharp contrast lines. This stress leads to the low diffraction contrast in TEM images. On the right side of TKD map black undefined areas correspond to beryllium oxide at the prior particle boundaries. These oxides have crystal structure and can be hardly distinguished from beryllide phase on TEM pictures. Fig. 11c shows a number of fine beryllium oxide particles of 20–50 nm in diameter in the Lamella 1 prepared across the prior particle boundaries. These homogeneously distributed fine oxide particles are also revealed on the polished surface of the lamella (Fig. 9b). The second lamella prepared from area free of coarse oxide particles has relatively coarser $Be_{12}Ti$ grains up to 2–2.5 μm in diameter and much smaller number of fine BeO particles (Fig. 11d).

The obtained data shows that after HIP at 1100°C $Be_{12}Ti$ phase has fine-grained microstructure with grains having 0.3–2.5 μm in diameter. Considering the high HIP temperature and the time of the treatment, it could be suggested that the obtained $Be_{12}Ti$ fine-grained structure has a considerable thermal stability at least at temperatures up to 1100°C. Apparently, the main reason

for this fact is the presence of numerous beryllium oxide precipitates in the matrix, especially near to the prior particle boundaries. These oxides are distributed along grain boundaries and could pin them, retarding the grains growth, and acting against recrystallization. Another reason for the small grain size of titanium beryllide might be the complexity of the reaction and diffusion process sequences during its formation. Indeed, according to the phase diagram (Fig. 1), pure titanium and pure beryllium have to react forming sequentially Be_2Ti, $Be_{13}Ti_2$, and $Be_{17}Ti_2$ intermediate beryllides close to titanium phase. At the same time, titanium has a negligible solubility in beryllium phase [9]. Therefore, formation of beryllide should begin by diffusion of beryllium atoms into titanium phase. In the end, 24 beryllium atoms and 2 titanium atoms have to arrange themselves to form $Be_{12}Ti$ crystal lattice. This means that a complete restructuring of the titanium phase occurs and no preferential orientation of titanium or beryllium can be inherit. A number of low-angle boundaries in some grains and the contrasting lines in the TEM pictures indicate high residual stresses. They likely to occur because of rapid cooling after HIP. This did not lead to cracking inside $Be_{12}Ti$ phase, but might result in its accommodative deformation. Nevertheless, fast cooling rates after HIP should be avoided, since beryllides of a different composition than $Be_{12}Ti$ could also cause cracking (Fig. 7d).

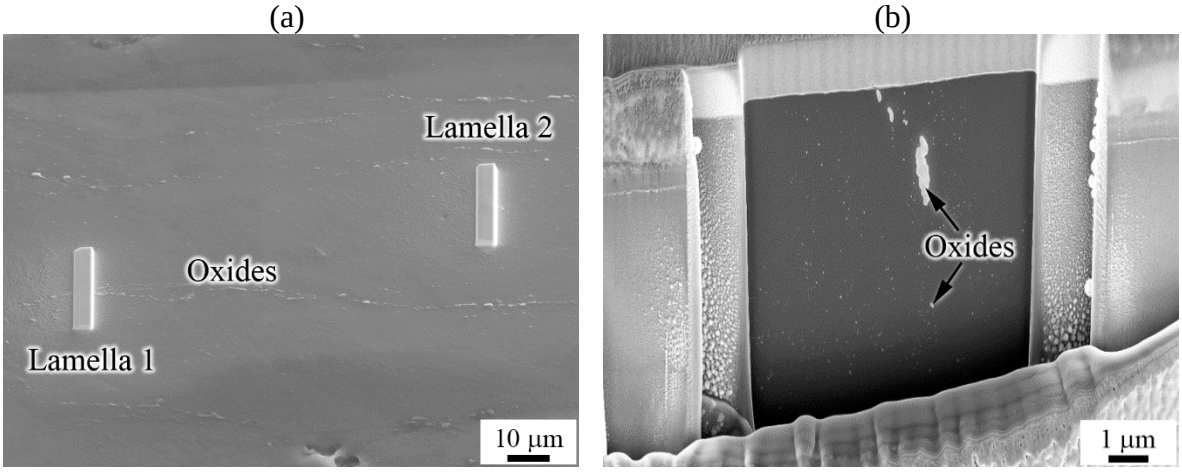

Fig. 9. (a) Pt-deposition before lamellae cutting procedure using FIB, (b) cross section of lamella 1 cut out across the prior particle boundary

ramil.gaisin@kit.edu

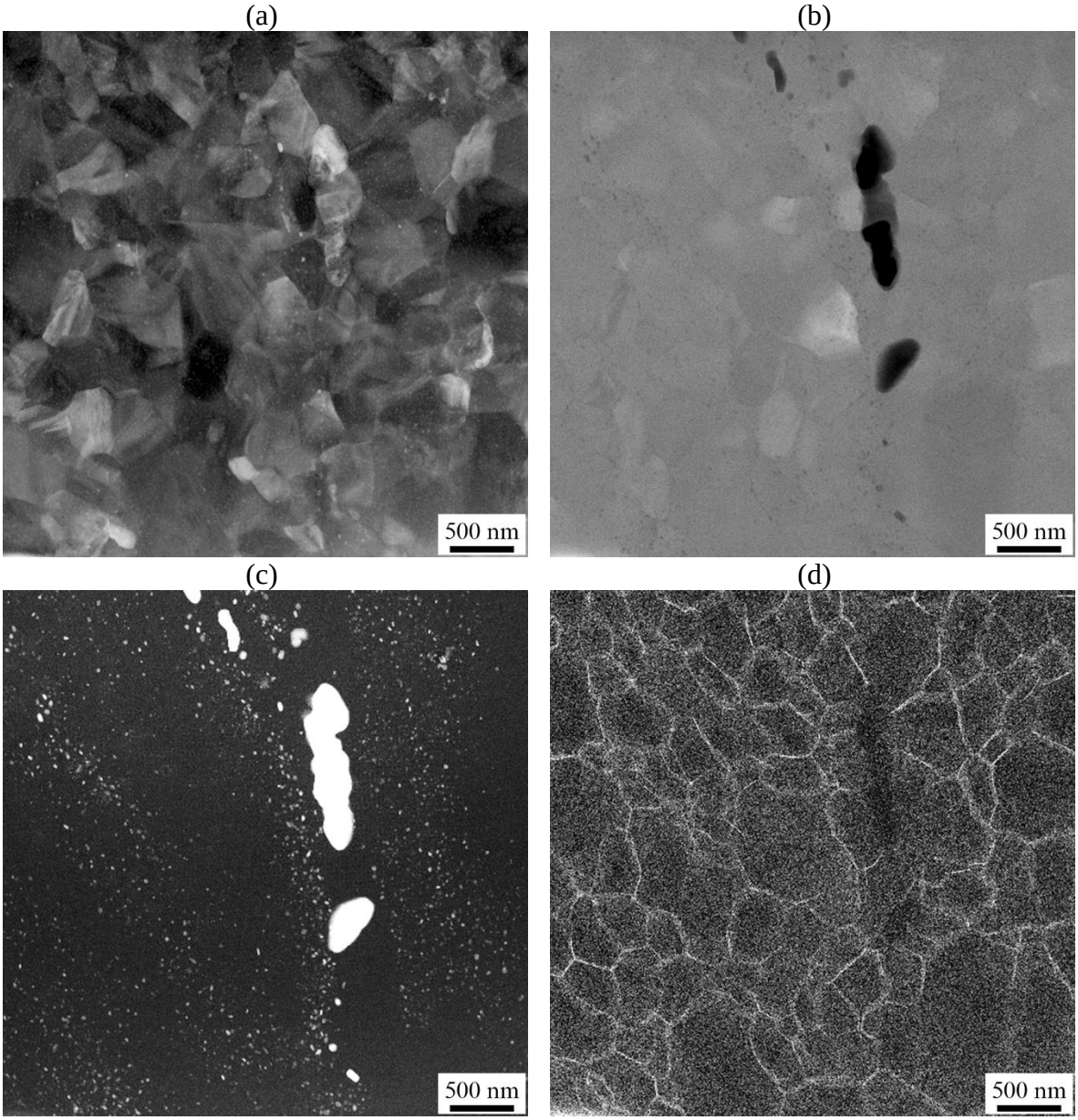

Fig. 10. (a) High-angle annular dark-field image and (b-d) elemental EDS maps of Be-Ti composite after extrusion and hot isostatic pressing: (b) titanium, (c) oxygen, (d) iron distributions. TEM of lamella 1

Microhardness measurements showed that intermetallic $Be_{12}Ti$ in the composite after HIP has a very high hardness, reaching 1420±40 HV (Table 2). Beryllium phase (together with pores) in the composite after HIP has a much lower microhardness of 360±30 HV. Considering the uncertainty of the measurement, the hardness of beryllium phase did not change after the last treatment. The obtained very high microhardness of $Be_{12}Ti$ is comparable to the hardness of topaz (≈1400 HV) and higher than the hardness of ZrO_2 (≈1300 HV) or martensite in steels (<1000 HV). It is also higher than hardness of arc melted $Be_{12}Ti$ and $Be_{10}Ti$ mixture (980±140HV, Table 2), $Be_{12}Ti$ prepared by vacuum hot pressing (960 HV in [9, 24]) and by plasma-sintering (≈1250 HV

in [3, 16]). The latter can be explained by grain boundary strengthening owing to small grain size and residual stresses after HIP.

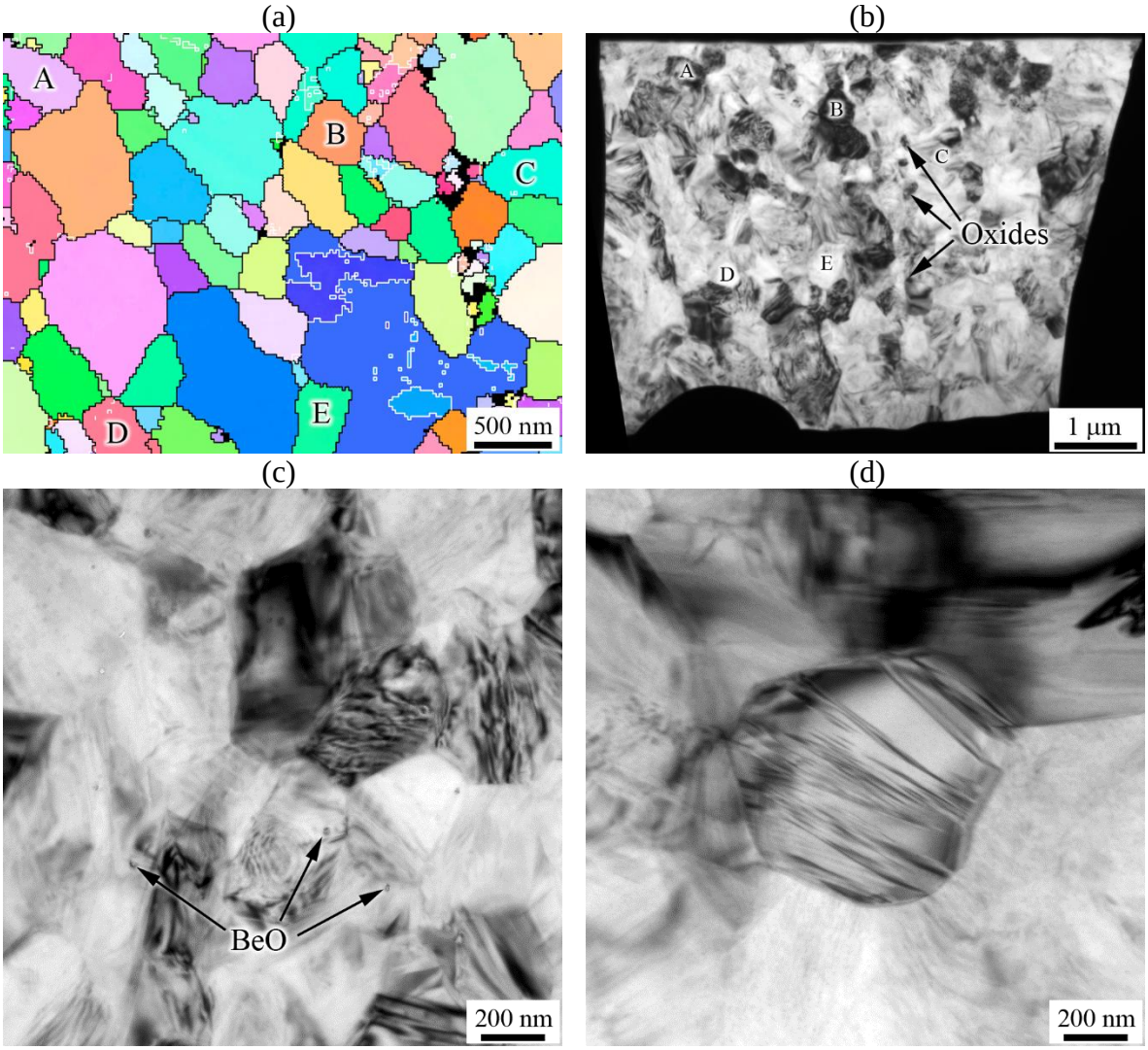

Fig. 11. Microstructure of Be-Ti composite: (a-c) cut out across the prior particle boundary, (d) cut out far from the prior particle boundary; (a) TKD map, (b) TEM panoramic view, (c-d) TEM micrographs; (a-c) lamella 1, (d) lamella 2. Black areas on the TKD map correspond to beryllium oxide particles on prior particle boundaries. The same grains on (a) and (b) are marked with capital letters.

Fig. 12 shows SEM micrograph of indentation imprints with cracks diverging from the centers of imprints. Such behavior during hardness measurement is characteristic of brittle materials. In [28-29] fracture toughness of $Be_{12}V$ and $Be_{17}Nb_2$ was estimated from the microhardness indentation tests and were found to be 0.84 and 1.1 $MPa \cdot m^{1/2}$ respectively. For $Be_{12}Nb$ fracture toughness was calculated somewhat higher up to 4 $MPa \cdot m^{1/2}$, which was explained by enhanced dislocation mobility [9]. In the present work, we used the same method of fracture toughness estimating via microhardness measurements as in the papers [28-30].

ramil.gaisin@kit.edu

To do this, the following formula was used:

$$K_c = \xi \cdot P\, C_0^{-3/2}\, (E/H)^{1/2} \quad (1)$$

where K_c is the fracture toughness, ξ is a constant, E is the elasticity modulus, H is the hardness, P is the load, and C_0 is the crack length from the center of the indentation.

Assuming $\xi = 0.016$ [30], $E = 280$ GPa [6], the fracture toughness of $Be_{12}Ti$ is calculated to be 2.4±0.3 MPa·m$^{1/2}$ at different loads of microhardness measurements. Thus, the value of fracture toughness turned out to be between values, obtained for other $Be_{12}Me$ beryllides such as $Be_{12}V$ and $Be_{12}Nb$. The value obtained for $Be_{12}Ti$ is greater than that of amorphous glasses (0.7–0.9 MPa·m$^{1/2}$), is close to the values of the fracture toughness of many ceramics, such as Al_2O_3, Si_3N_4, SiC (2.1–4.9 MPa·m$^{1/2}$) and less than that of beryllium with 10–15 MPa·m$^{1/2}$ [9, 27, 30].

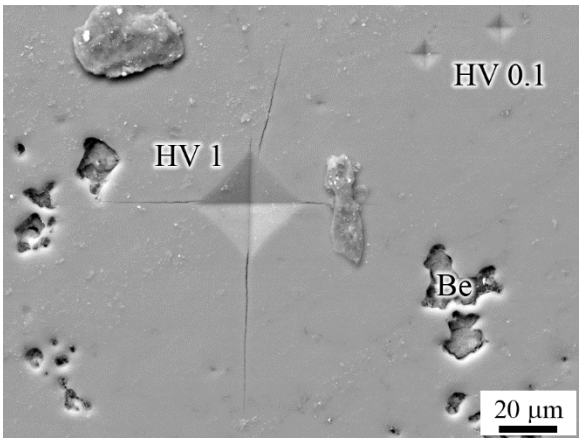

Fig. 12. SEM micrographs of indentation imprints produced with 1 kgf (HV1) and 100 gf (HV0.1) loads showing the cracking of $Be_{12}Ti$ phase

The obtained fine-grained structure of $Be_{12}Ti$ after extrusion and HIP could have attractive properties under irradiation. It should have high thermal stability at temperatures up to 1100°C while the expected working temperature of $Be_{12}Ti$ is lower than 1000°C. It is assumed that a large number of grain boundaries owing to the small grain size will retain low amount of tritium. The grain boundaries are effective sinks of lattice defects such as vacancies, interstitials, helium and tritium atoms and, thus, the required path from the center of the grain to the boundary is reduced. On the other hand, the remained beryllium phase can still retain considerable amount of tritium, therefore the HIP regimes should be refined in order to minimize the beryllium phase volume fraction.

4. Conclusions

Intermetallic $Be_{12}Ti$ phase was obtained using conventional casting or hot isostatic pressing (HIP) starting from the extruded Be-Ti composite rods. Owing to intense beryllium evaporation and composition shift towards titanium, arc melting resulted in two phase $Be_{12}Ti$ and $Be_{10}Ti$ microstructure with considerable porosity and shrinkage in the ingot. In the case of extrusion and HIP at 1100°C, $Be_{12}Ti$ is synthesized with residue Be phase and trace BeO on the prior particle boundaries. TEM demonstrated that fine BeO particles are often distributed along $Be_{12}Ti$ grain boundaries and can pin them. According to EBSD and TKD analyses, even after high-temperature

HIP treatment $Be_{12}Ti$ has relatively small grain size of 0.3–2.5 μm depending on the distance from the prior particle boundaries. $Be_{12}Ti$ phase after HIP has high microhardness up to 1420 HV and fracture toughness of about 2.4 $MPa \cdot m^{1/2}$. The powder metallurgy route, including powder extrusion and HIP, was chosen for further research in order to manufacture $Be_{12}Ti$ neutron multiplier blocks manufacturing for DEMO fusion reactor.

Acknowledgements
This work has been carried out within the framework of the EUROfusion Consortium and has received funding from the Euratom research and training programme 2014–2018 and 2019–2020 under grant agreement No 633053. The views and opinions expressed herein do not necessarily reflect those of the European Commission. The work was partly accomplished according to the state assignment of IMSP RAS [AAAA-A17-117041310215-4]. The authors gratefully acknowledge V. Kuksenko and J. Claridge (UK Atomic Energy Authority, Culham Science Centre) for their assistance with the FIB sample preparation.

References

[1] F.A. Hernández, P. Pereslavtsev, G. Zhou, B. Kiss, Q. Kang, H. Neuberger, V. Chakin, R. Gaisin, P. Vladimirov, L.V. Boccaccini, G.A. Spagnuolo, S. D'Amico, I. Moscato, Advancements in the Helium-Cooled Pebble Bed Breeding Blanket for the EU DEMO: Holistic Design Approach and Lessons Learned, Fusion Science and Technology 75 (2019) 352–364.

[2] H. Kawamura, E. Ishitsuka, K. Tsuchiya, M. Nakamichi, M. Uchida, H. Yamada, K. Nakamura, H. Ito, T. Nakazawa, H. Takahashi, S. Tanaka, N. Yoshida, S. Kato, Y. Ito, Development of advanced blanket materials for a solid breeder blanket of a fusion reactor, Nuclear Fusion 43 (2003) 675–680.

[3] J.-H. Kim, M. Nakamichi, Comparative study on arc-melted and plasma-sintered beryllides, Journal of Alloys and Compounds 546 (2013) 171–175.

[4] J. Shimwell, L. Lu, Y. Qiu, P. Pereslavtsev, A. Häußler, F. Hernández, C. Zeile, T. Eade, G.A Spagnuolo, S. McIntosh, L. Packer, T. Barrett, Automated parametric neutronics analysis of the Helium Cooled Pebble Bed breeder blanket with Be12Ti, Fusion Engineering and Design 124 (2017) 940–943.

[5] Y. Mishima, N. Yoshida, H. Kawamura, K. Ishida, Y. Hatano, T. Shibayama, K. Munakata, Y. Sato, M. Uchida, K. Tsuchiya, S. Tanaka, Recent results on beryllium and beryllides in Japan, Journal of Nuclear Materials 367-370 (2007) 1382–1386.

[6] D.V. Bachurin, P.V. Vladimirov, Ab initio study of Be and $Be_{12}Ti$ for fusion applications, Intermetallics 100 (2018) 163–170.

[7] G. V. Samsonov and I. M. Vinitskii, Handbook of Refractory Compounds (translated from the Russian by Kenneth Shaw). IFI/Plenum Press, New York, 1980.

[8] J. Reimann, G. Piazza, H. Harsch, Thermal conductivity of compressed beryllium pebble beds, Fusion Engineering and Design 81 (2006) 449–454.

[9] K.A. Walsh, Beryllium Chemistry and Processing, ASM International, 2009.

[10] L.A. Jacobson, R.J. Hanrahan Jr., J.L. Smith, Beryllides, in: Intermetallic Compounds - Principles and Practice, John Wiley & Sons, Ltd, 2002, pp. 37–51.

[11] M. Uchida, H. Kawamura, M. Uda, Y. Ito, Elementary development for beryllide pebble fabrication by rotating electrode method, Fusion Engineering and Design 69 (2003) 491–498.

ramil.gaisin@kit.edu

[12] J.-H. Kim, M. Nakamichi, The effect of sintering time on synthesis of plasma sintered beryllides, Journal of Nuclear Materials 442 (2013) S461 - S464.
[13] J.-H. Kim, M. Nakamichi, Sinterability and mechanical properties of plasma-sintered beryllides with different Ti contents, Journal of Alloys and Compounds 556 (2013) 292–295.
[14] J.-H. Kim, M. Nakamichi, Optimization of synthesis conditions for plasma-sintered beryllium–titanium intermetallic compounds, Journal of Alloys and Compounds 577 (2013) 90–96.
[15] J.-H. Kim, M. Miyamoto, Y. Hujii, M. Nakamichi, Reactivity and deuterium retention properties of titanium-beryllium intermetallic compounds, Intermetallics 82 (2017) 20–25.
[16] V.M. Imayev, R.A. Gaisin, R.M. Imayev, Microstructure and mechanical properties of near α titanium alloy based composites prepared in situ by casting and subjected to multiple hot forging, Journal of Alloys and Compounds 762 (2018) 555–564.
[17] P. Kurinskiy, H. Leiste, A. Goraieb, R. Rolli, S. Mueller, J. Reimann, A. Moeslang, Production of Be-Ti and Be-Zr rods by extrusion and their characterization, Fusion Engineering and Design 136 (2018) 49–52.
[18] Murray, J.L., 1987. Beryllium-Titanium Phase Diagram, Phase Diagrams of Binary Beryllium Alloys, ASM International
[19] J.M. Beeston, G.R. Longhurst, R.S. Wallace, S.P. Abeln, Mechanical properties of irradiated beryllium, Journal of Nuclear Materials 195 (1992) 102–108.
[20] C. Leyens, M. Peters, Titanium and Titanium Alloys, Fundamentals and Applications, Weinheim, Germany, 2003.
[21] B. Sun, S. Li, H. Imai, J. Umeda, K. Katsuyoshi, Oxygen Solid Solution Strengthened Pure Tiatanium Powder Materials, Transactions of JWRI 41 (2012) 59–64
[22] H. Okamoto, Be-Ti (Beryllium-Titanium), Journal of Phase Equilibria and Diffusion 29 (2008) 202.
[23] V. Chakin, R. Rolli, R. Gaisin, P. Kurinskiy, J.-H. Kim, M. Nakamichi, Effect of heat treatment of titanium beryllide on tritium/hydrogen release, Fusion Engineering and Design 137 (2018) 165–171.
[24] S.M. Bruemmer, B.W. Arey, J.L. Brimhall, J.P. Hirth, Hot-hardness comparisons among isostructural $Be_{12}X$ intermetallic compounds, J. Mater. Res. 8, 7 (1993) 1550–1557.
[25] P. Kurinskiy, A. Moeslang, M. Klimiankou, A.A. Goraieb, H. Harsch, Manufacturing methods and characterisation of titanium beryllides, Fusion Engineering and Design 82 (2007) 2353–2358.
[26] P. Kurinskiy, V. Chakin, A. Moeslang, R. Rolli, A.A. Goraieb, H. Harsch, E. Alves, N. Franco, Characterisation of titanium beryllides with different microstructure, Fusion Engineering and Design 84 (2009) 1136–1139.
[27] M. Nakamichi, K. Yonehara, Sintering properties of beryllides for advanced neutron multipliers, Journal of Nuclear Materials 417 (2011) 765–768.
[28] T.G. Nieh, J. Wadsworth, F.C. Grensing, J.-M. Yang, Mechanical properties of vanadium beryllide, VBe12, Journal of Materials Science 27 (1992) 2660–2664.
[29] T.G. Nieh, J. Wadsworth, T.C. Chou, D. Owen, A.H. Chokshi, Creep of a niobium beryllide, Nb_2Be_{17}, Journal of Materials Research 8 (1993) 757–763.
[30] G.R. Anstis, P. Chantikul, B.R. Lawn, D.B. Marshall, A Critical Evaluation of Indentation Techniques for Measuring Fracture Toughness: I, Direct Crack Measurements, Journal of the American Ceramic Society 64 (1981) 533–538.